Observational Evidence for Black Holes

Ramesh Narayan and Jeffrey E. McClintock

Harvard Smithsonian Center for Astrophysics
60 Garden Street, Cambridge, MA 02138, U.S.A.

1

Observational Evidence for Black Holes

Abstract

Astronomers have discovered two populations of black holes: (i) stellar-mass black holes with masses in the range 5 to 30 solar masses, millions of which are present in each galaxy in the universe, and (ii) supermassive black holes with masses in the range 10^6 to 10^{10} solar masses, one each in the nucleus of every galaxy. There is strong circumstantial evidence that all these objects are true black holes with event horizons. The measured masses of supermassive black holes are strongly correlated with properties of their host galaxies, suggesting that these black holes, although extremely small in size, have a strong influence on the formation and evolution of entire galaxies. Spin parameters have recently been measured for a number of black holes. Based on the data, there is an indication that the kinetic power of at least one class of relativistic jet ejected from accreting black holes may be correlated with black hole spin. If verified, it would suggest that these jets are powered by a generalized Penrose process mediated by magnetic fields.

1.1 Historical Introduction

The first astrophysical black hole to be discovered was Cygnus A, which stood out already as a bright localized radio source in the pioneering radio sky map of Grote Reber [60, 32]. The recognition that Cyg A is a black hole, however, had to wait a few decades. It required identifying the source with a distant galaxy [72, 2]; resolving its radio image into a pair of radio lobes [34] with a compact source at the center [30] (Fig. 1.1); the discovery of quasars [67]; and the growing realization that all of these objects require an extremely powerful but extraordinarily compact engine. The only plausible
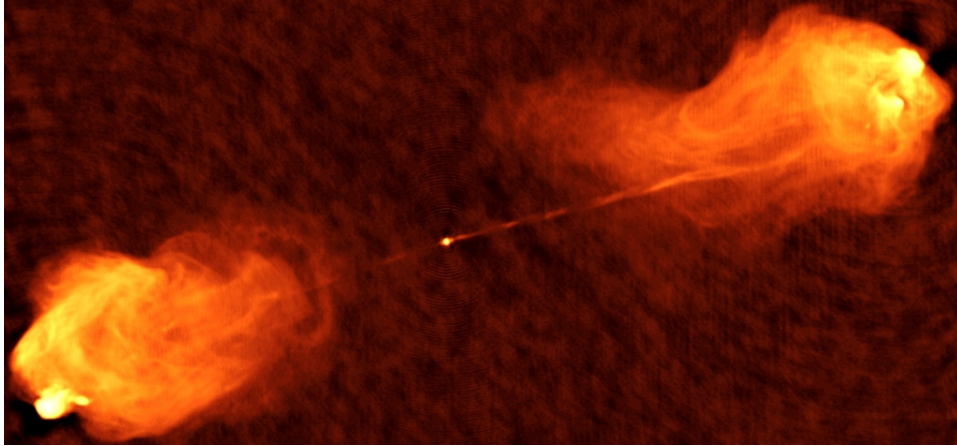
Figure 1.1 A modern radio image of Cyg A. The compact bright dot at the center of the image is the presumed supermassive black hole located in the nucleus of a giant elliptical galaxy. The two broken lines extending out on either side are relativistic jets carrying enormous amounts of energy in twin collimated beams. The jets are stopped by the intergalactic medium and then spread out into two giant lobes. All the observed radio emission is due to synchrotron radiation from relativistic electrons spiraling in magnetic fields. (Figure courtesy of C. Carilli and R. Perley, NRAO.)

explanation is that Cyg A, like quasars and other active galactic nuclei (AGN), is powered by a supermassive black hole.

The first stellar-mass black hole to be discovered was Cyg X–1 (also, co-incidentally, in the constellation of Cygnus), which was catalogued in the early days of X-ray astronomy as a bright X-ray point source [7]. Evidence of its black hole nature came relatively soon. The optical counterpart was confirmed to be a 5.6-day binary star system in our Galaxy [77], and dynamical observations of the stellar component showed that Cyg X–1 has a mass of at least several solar masses [6, 81], making it too massive to be a neutron star. It was therefore recognized as a black hole.

Cyg A and Cyg X–1 are members of two large but distinct populations of black holes in the universe. We briefly review our current knowledge of the two populations, and summarize the reasons for identifying their members as black holes.

1.2 Supermassive Black Holes

1.2.1 Mass and Size Estimates

The radiation we see from supermassive black holes is produced by accretion, the process by which gas spirals into the black hole from a large radius. As the gas falls into the potential well, it converts a part of the released potential energy to thermal energy, and ultimately into radiation. A characteristic luminosity of any gravitating object is the Eddington limit at which outward radiative acceleration is balanced by the inward pull of gravity:

$$L_{\mathrm{E}} = \frac{4\pi G M m_p c}{\sigma_T} = 1.25 \times 10^{38} \frac{M}{M_\odot} \ \mathrm{erg\,s^{-1}}, \qquad (1.1)$$

where M is the mass of the object, $M_\odot = 1.99 \times 10^{33}$ g is the mass of the Sun, m_p is the mass of the proton, and $\sigma_T = 6.65 \times 10^{-25}$ cm^2 is the Thomson cross-section for electron scattering. A spherical object in equilibrium cannot have a luminosity $L > L_{\mathrm{E}}$. Since bright quasars have typical luminosities $L \sim 10^{46}$ erg s^{-1}, they must thus be very massive: $M > 10^8 M_\odot$.

A large mass by itself does not indicate that an object is a black hole. The second piece of information needed is its size. In the case of quasars and other AGN, a number of observations indicate that their sizes are not very much larger than the gravitational radius of a black hole of mass M:

$$R_g = \frac{GM}{c^2} = 1.48 \times 10^5 \frac{M}{M_\odot} \ \mathrm{cm}. \qquad (1.2)$$

The earliest indication for a small size came from the fact that quasars show noticeable variability on a time scale of days. Since an object cannot have large-amplitude variations on a time scale shorter than its light-crossing time, it was deduced that quasars are no more than a light-day across, i.e., their sizes must be $< 10^2 R_g$.

Modern limits are tighter. For instance, gravitational microlensing observations of the quasar RXJ 1131–1231 indicate that the X-ray emission comes from a region of size $\sim 10 R_g$ [12]. Tighter and more direct limits ($<$ few R_g) are obtained from observations of the Kα line of iron, which show that gas orbits the central object at a good fraction of the speed of light [76, 16]. The only astrophysically plausible object satisfying these mass and size limits is a supermassive black hole.

1.2.2 The Mass of Sagittarius A*

Quasars are too distant for direct measurements of their mass. The situation is more favorable for supermassive black holes in the nuclei of nearby
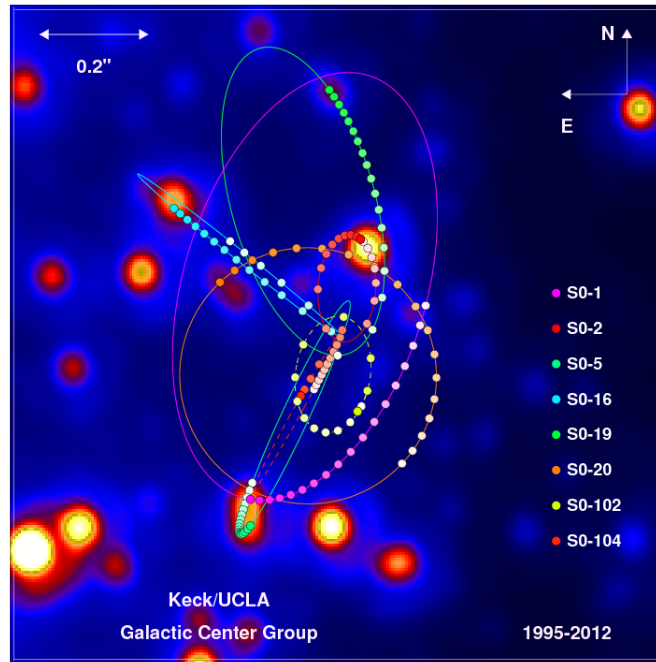
Figure 1.2 Orbital tracks on the plane of the sky over the period 1995–2012 of 8 bright stars (S0–1, S0–2, ... , S0–104) at the center of our Galaxy. Keplerian fits to these orbits give the position and mass of the supermassive black hole in the nucleus of the Galaxy. (Figure courtesy of A. Ghez and her research team at UCLA, based on data obtained with the W. M. Keck Telescopes.)

galaxies. The majority of these black holes have very low accretion luminosities and are thus very dim. This is an advantage. Without the glare of a bright central source, it is possible to carry out high resolution imaging and spectroscopic observations relatively close to the black hole and thereby estimate the black hole mass via dynamical methods. The most spectacular results have been obtained in our own Milky Way Galaxy.

Over the past twenty years, two different groups have successfully used the largest telescopes on Earth to obtain diffraction-limited infrared images of our Galactic Center, and have thereby mapped the trajectories of stars orbiting the Galactic nucleus. Remarkably, all the stars move on Keplerian orbits around a common focus [68, 24] (see Fig. 1.2) containing a dark mass of $4.4 \pm 0.4 \times 10^6 M_\odot$ [46]. Since the dark mass must be interior to the pericenter of the most compact stellar orbit, its radius must be $< 10^3 R_g$.

In fact, a much tighter limit can be placed on the size. At the center of

our Galaxy is a radio source called Sagittarius A* (Sgr A*). This source has been shown to be essentially at rest with respect to the Galaxy, moving with a speed less than about $1\,\mathrm{km\,s^{-1}}$ [61]. Given the huge velocities of stars orbiting in its vicinity (the fastest stars mentioned in the previous paragraph move with speeds up to $10^4\,\mathrm{km\,s^{-1}}$), equipartition arguments imply that Sgr A* must be more massive than $10^5 M_\odot$. The only plausible interpretation is that Sgr A* is identical to the $4.4 \times 10^6 M_\odot$ object inferred from stellar orbits.

Meanwhile, Sgr A* is a bright radio source and has been imaged with exquisite precision using interferometric techniques. The most recent observations indicate that emission at $1.3\,\mathrm{mm}$ wavelength comes from within a radius of a few R_g [14, 22]. This robust size constraint makes it virtually certain that Sgr A* must be a supermassive black hole.

1.2.3 Other Nearby Supermassive Black Holes

Occasionally, the orbiting gas in the accretion disk around a supermassive black hole produces radio maser emission from transitions of the water molecule. If the galaxy is sufficiently nearby, the maser emitting "blobs" can be spatially resolved by interferometric methods and their line-of-sight velocities can be measured accurately by the Doppler technique. The most spectacular example is the nearly edge-on disk in the nucleus of the galaxy NGC 4258 [48, 29], where the measured velocities follow a perfect Keplerian profile. The required black hole mass is $4.00 \pm 0.09 \times 10^7 M_\odot$ [33].

Maser disks are relatively rare. A more widely used method employs high spatial resolution observations in the optical band with the Hubble Space Telescope (see [39] for a comprehensive review). By simultaneously fitting the spatial brightness distribution and two-dimensional line-of-sight velocity distribution of stars in the vicinity of a galactic nucleus, and using advanced three-integral dynamical models for stellar orbits, it is possible to estimate the mass of a compact central object, if one is present. Several tens of black hole masses have been measured by this method, with uncertainties typically at about a factor of two. In the majority of cases, models without a compact central mass are ruled out with high statistical significance. From these studies it has become clear that essentially every galaxy in the universe hosts a supermassive black hole in its nucleus.

Other less direct methods are available for measuring masses of more distant black holes. Two methods in particular, one based on reverberation mapping [59] and the other on an empirical linewidth-luminosity relation [80], deserve mention.
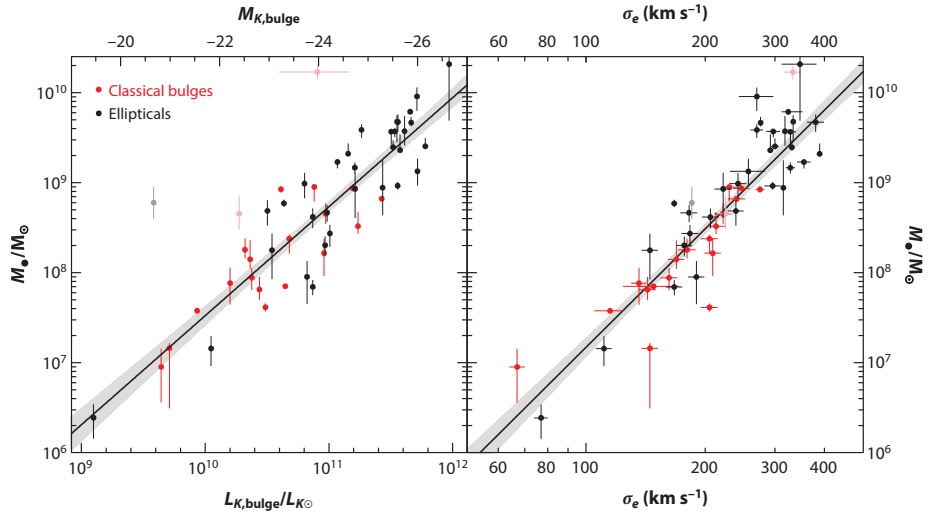
Figure 1.3 Observed correlations between supermassive black hole mass $M_\bullet$ and (left) the infrared luminosity of the bulge of the host galaxy in units of solar luminosities (represented in the top axis by the absolute magnitude $M_{\text{K,bulge}}$), and (right) the velocity dispersion σ_e of the stars in the bulge. (Reprinted with permission from [39].)

1.2.4 A Remarkable Correlation

Unquestionably, the most dramatic discovery to come out of the work described in the previous subsection is the fact that supermassive black hole masses are correlated strongly with the properties of their host galaxies. Figure 1.3 (from [39]) shows two such correlations: (a) between the black hole mass M and the luminosity (in this case infrared luminosity) of the bulge of the galaxy [42], and (b) between M and the stellar velocity dispersion σ_e of the bulge [21, 23].

At first sight, these correlations are baffling. The mass of the black hole is typically 10^3 times smaller than that of the bulge, and its size (R_g) is 10^8 times smaller. How could such an insignificant object show such a strong correlation with its parent galaxy? The answer can be understood by considering a more relevant quantity than either mass or radius alone: the binding energy GM^2/R. In terms of binding energy, the black hole is actually "stronger" (by quite a bit) than the entire galaxy. Indeed, the current paradigm, and a major area of research, is that supermassive black holes exert considerable "feedback" on their host galaxies during the formation and growth of both entities. As a natural consequence, their parameters become strongly correlated in the manner shown in Fig. 1.3 (e.g. [13, 37, 38]).

As an important practical application, the above correlations can be used to estimate the masses of high redshift black holes using the luminosities or stellar velocity distributions of their host galaxies.

1.3 Stellar-Mass Black Holes

Many millions of stellar-mass black holes are inferred to be present in our Milky Way galaxy, and in every other galaxy in the universe, but the existence of only 24 of them has been confirmed via dynamical observations. These 24, whose masses are in the range $M = 5 - 30 \ M_\odot$, are located in X-ray binary systems, 21 of which are sketched to scale in Fig. 1.4. The X-rays are produced by gas that flows from the companion star on to the black hole via an accretion disk. Close to the black hole (radii $\sim 10 R_g$), the accreting gas reaches a typical temperature of $\sim 10^7$ K and emits X-rays.

The 24 black hole binaries divide naturally into two classes: (i) 5 of these black holes are *persistent* X-ray sources, which are fed by winds from their massive companion stars. (ii) The remaining 19 binaries are *transient* sources, whose X-ray luminosities vary widely, ranging from roughly the Eddington luminosity L_E down to as low as $\sim 10^{-8} L_E$. A typical transient black hole is active for about a year and then remains quiescent for decades.

1.3.1 Mass Measurements

The masses of stellar-mass black holes are measured by employing the same methodologies that have been used for over a century to measure the masses of ordinary stars in binary system. Most important is the radial velocity curve of the companion star, which is derived from a collection of spectroscopic observations that span an orbital cycle. These velocity data deliver two key parameters: the orbital period P and the semi-amplitude of the velocity curve K, which in turn determine the value of the mass function:

$$f(M) \equiv \frac{PK^3}{2\pi G} = \frac{M \sin^3 i}{(1+q)^2}, \tag{1.3}$$

where i is the orbital inclination angle of the binary (Fig. 1.4) and q is the ratio of the companion star mass to that of the black hole.

An inspection of the above equation shows that the value of the observable $PK^3/2\pi G$, which can be accurately measured, is the absolute minimum mass of the black hole. For ten out of the total sample of 24 stellar-mass black holes, this minimum mass ranges from $3 - 8 \ M_\odot$ (see Table 2 in [56] and [73]). In comparison, the maximum stable mass of a neutron star is
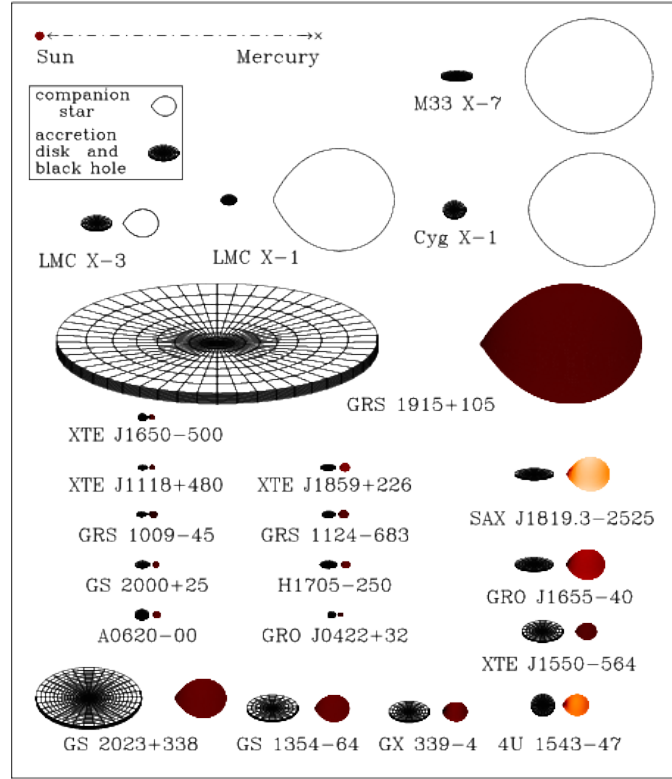
Figure 1.4 Sketches of 21 black hole binaries (see scale and legend in the upper-left corner). The tidally-distorted shapes of the companion stars are accurately rendered in Roche geometry. The black holes are located at the centers of the disks. A disk's tilt indicates the inclination angle i of the binary, where $i = 0$ corresponds to a system that is viewed face-on; e.g., $i = 21°$ for 4U 1543–47 (bottom right) and $i = 75°$ for M33 X–7 (top right). The size of a system is largely set by the orbital period, which ranges from 33.9 days for the giant system GRS 1915+105 to 0.2 days for tiny XTE J1118+480. Three systems hosting persistent X-ray sources — M33 X–7, LMC X–1 and Cyg X–1 — are located at the top. The other 18 systems are transient sources. (Figure courtesy of J. Orosz.)

widely agreed to be less than about 3 $M_\odot$ [64, 36]. Therefore, on the basis of a single robust observable, one can conclude that these ten compact X-ray sources must be black holes.

In order to obtain the actual masses of these and other stellar-mass black holes, one must additionally determine q and i. The mass ratio q is usually estimated by measuring the rotational velocity of the companion star. The inclination angle i can be constrained in several ways; commonly, one models the light curve of the tidally-distorted companion star. Selected mass mea-

Table 1.1 *Masses and spins, determined via the continuum-fitting method, for a selected sample of seven black holes. By the No-Hair Theorem (§1.4.3), the data constitute complete descriptions of these black holes[a].*

System	$M/M_\odot$	a_*	References
Persistent			
Cyg X–1	14.8 ± 1.0	> 0.95	[52]; [26]
LMC X–1	10.9 ± 1.4	$0.92^{+0.05}_{-0.07}$	[54]; [25]
M33 X–7	15.65 ± 1.45	0.84 ± 0.05	[53]; [41]
Transient			
GRS 1915+105	10.1 ± 0.6	$> 0.95^b$	[73]; [44]
GRO J1655–40	6.3 ± 0.5	0.70 ± 0.10^b	[28]; [70]
XTE J1550–564	9.1 ± 0.6	$0.34^{+0.20}_{-0.28}$	[55]; [75]
A0620–00	6.6 ± 0.25	0.12 ± 0.19	[9]; [27]

Notes:
[a] Errors are quoted at the 68% level of confidence, except for the two spin limits, which are estimated to be at the 99.7% level of confidence.
[b] Uncertainties are greater than those in papers cited because early error estimates were crude.

surements for seven black holes are given in Table 1.1. For further details on measuring the masses of black holes, see the references cited in the table and [10].

1.3.2 Spin Estimates

Spin is difficult to measure because its effects manifest only near the black hole ($R < 10R_g$). One must not only make discerning observations in this tiny region of space-time, but one must also have a reliable model of the accretion flow in strong gravity. Two fortunate circumstances come to the rescue: (i) We do have at least one simple black hole accretion model, viz., the thin accretion disk model [71, 51]. (ii) Among the several distinct and long-lived accretion states observed in individual stellar-mass black holes [62], one particularly simple state, called the *thermal* state, is dominated by emission from an optically thick accretion disk, and is well-described by the thin disk model.

According to the thin disk model, the inner edge of the accretion disk is located at the radius of the innermost stable circular orbit R_{ISCO}. Moreover, R_{ISCO}/R_g is a monotonic function of the dimensionless black hole spin pa-

rameter $a_* = cJ/GM^2$ [4], where J is the angular momentum of the black hole (note, $|a_*| < 1$). In the continuum-fitting method of measuring spin [82, 70, 44], one observes radiation from the accreting black hole when it is in the thermal state. One then estimates $R_{\rm ISCO}$, and hence a_*, by fitting the thermal continuum spectrum to the thin-disk model. The method is simple: It is strictly analogous to using the theory of blackbody radiation to measure the radius of a star whose flux, temperature and distance are known. By this analogy, it is clear that to measure $R_{\rm ISCO}$ one must measure the flux and temperature of the radiation from the accretion disk, which one obtains from X-ray observations. One must also measure the source distance D and the disk inclination i (an extra parameter that is not needed for a spherical star). Additionally, one must know M in order to scale $R_{\rm ISCO}$ by R_g to determine a_*. The uncertainties in all these ancilliary measurements contribute to the overall error budget.

The spins of ten black holes have been measured by the continuum-fitting method, seven of which are presented in Table 1.1. The robustness of the method is demonstrated by the dozens or hundreds of independent and consistent measurements of spin that have been obtained for several black holes, and through careful consideration of many sources of systematic error. For a review of the continuum-fitting method and a summary of results, see [43].

An alternative method of measuring black hole spin, in which one determines $R_{\rm ISCO}/R_g$ by modeling the profile of the broad and skewed fluorescence Fe Kα line, has been widely practiced since its inception [17]. However, obtaining reliable results for stellar-mass black holes is challenging because one must use data in states other than the thermal state, where the disk emission is strongly Comptonized and harder to model. Furthermore, the basic geometry of the disk is poorly constrained, and it is even doubtful that the inner edge of the disk is located at $R_{\rm ISCO}$.

To date, the Fe-line method has been used to estimate the spins of more than a dozen stellar-mass black holes. A few of these black holes have been studied using both the continuum-fitting and Fe-line methods, and there is reasonable agreement between the two independent spin estimates. The Fe-line method is especially important in the case of supermassive black holes [63], where it is difficult to apply the continuum-fitting method.

1.3.3 Intermediate Mass Black Holes

Are there black holes of intermediate mass, i.e., black holes that are too massive ($M > 100\ M_\odot$) to have formed from ordinary stars but, at the

same time, are not in the nucleus of a galaxy? Such objects, referred to as intermediate mass black holes (IMBHs), would represent a new and distinct class of black hole. The leading IMBH candidates are the brightest "ultra-luminous" X-ray sources in external galaxies, whose observed luminosities can be up to $\sim 100 - 1000$ times the Eddington luminosity of a $10 M_\odot$ black hole. Although there are some promising candidates (e.g. [20, 11]), none has been confirmed because of the difficulties of obtaining a firm dynamical measurement of mass.

1.4 Physics of Astrophysical Black Holes

1.4.1 Are They Really Black Holes?

The astrophysical black holes discussed so far are technically only black hole candidates. True, they are sufficiently massive and compact that we cannot match the observations with any object in stable equilibrium other than a black hole. However, this by itself does not prove that the objects are true black holes, defined as objects with event horizons. Black hole candidates could, in principle, be exotic objects made of some kind of unusual matter that enables them to have a surface (no horizon), despite their extreme compactness.

Astronomers have devised a number of tests to check whether black hole candidates have a "surface". In brief, all the evidence to date shows that black hole candidates do not have normal surfaces that are visible to distant observers (see [49, 8]; and references therein). The arguments are sufficiently strong that — barring scenarios that are more bizarre than a black hole — they essentially "prove" that the astrophysical black hole candidates discussed in this article possess event horizons. However, the proof is still indirect [1].

1.4.2 Spinning Black Holes and the Penrose Process

It is a remarkable consequence of black hole theory that a spinning black hole has free energy available to be tapped. Penrose [58] showed via a simple toy model that particles falling into a spinning hole on negative energy orbits can extract some of the black hole's spin energy. Energy extraction is allowed by the Area Theorem, which states that the horizon area A of a black hole cannot decrease with time: $dA/dt \geq 0$ (e.g., [3]). For a black hole of mass M and dimensionless spin a_*, the area is given by $A = 8\pi R_g^2 [1 + (1 - a_*^2)^{1/2}]$. Therefore, a black hole can lose energy and mass, and thus reduce

the magnitude of R_g, provided the spin parameter a_* also decreases by a sufficient amount to satisfy the Area Theorem. In effect, the hole spins down and gives up some of its spin-energy to infinity. Penrose's negative energy particles are a conceptually transparent way of demonstrating this effect.

An astrophysically more promising scenario for the extraction of spin energy makes use of magnetized accretion flows, as outlined in early papers [65, 5]. In this mechanism, the dragging of space-time by a spinning hole causes magnetic field lines to be twisted, resulting in an outflow of energy and angular momentum along field lines. Does this actually happen anywhere in the universe? Astronomers have long hypothesized that relativistic jets such as those in Cygnus A (Fig. 1.1) might be explained by some such process.

In recent years, general relativistic magnetohydrodynamic (MHD) numerical simulations of accreting spinning black holes have been carried out that show relativistic jets forming naturally from fairly generic initial conditions. More importantly, the simulations show unambiguously that, in at least some cases, the jet receives its power from the spin energy of the black hole and not from the accretion disk [78, 57, 40]. Specifically, energy and angular momentum flow directly from the black hole through the jet to the external universe, and the mass and spin of the black hole consequently decrease. The jet power varies approximately as a_*^2, and is thus largest for the most rapidly spinning holes. In brief, a generalized MHD version of the Penrose process operates naturally and efficiently in idealized simulations on a computer.

The observational situation is less clear. Radio-emitting relativistic jets have been known in AGN for many decades (e.g., Fig. 1.1), and more recently, jets have been discovered also in stellar-mass black holes (Fig. 1.5 shows a famous example). A very interesting relation has been found between the radio luminosity L_R, which measures jet power, the X-ray luminosity L_X, which measures accretion power, and the black hole mass M [45, 31, 18]. This relation, called the "fundamental plane of black hole activity" (Fig. 1.6), extends over many decades of the parameters, connecting the most massive and luminous AGN with stellar-mass black holes. The relatively tight correlation, which is further emphasized in recent work [79], implies that jet power depends primarily on the black hole mass and accretion rate, leaving little room for an additional dependence on black hole spin. However, most of the black holes plotted on the fundamental plane do not have spin measurements, so the argument for a lack of spin-dependence is somewhat indirect.

Meanwhile, tentative but direct observational evidence for a correlation between black hole spin and jet power has been found in a sample of stellar-
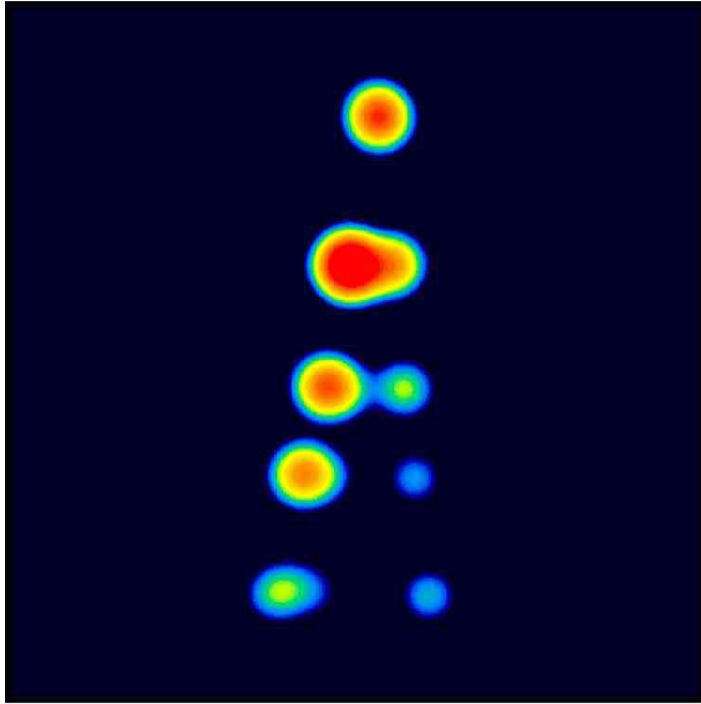
Figure 1.5 A sequence of radio images [47] of the transient black hole X-ray binary GRS 1915+105 during the period 18 March 1994 (uppermost image consisting of a single blob) to 16 April 1994 (lowermost image with two widely separated blobs). Two radio-emitting blobs were ejected from the source around the time of the first observation, and they subsequently moved ballistically outward from the source. The blob on the left has an apparent speed on the sky greater than the speed of light (superluminal motion), which is a relativistic effect. The Lorentz factor of each blob is estimated to be $\gamma \approx 2.6$. (Figure courtesy of F. Mirabel.)

mass black holes for which spins had been previously measured [50, 74] (Fig. 1.7). The evidence is still controversial [66, 43], in large part because of the small size of the sample. In addition, the correlation is restricted to stellar-mass black holes that accrete at close to the Eddington limit and produce so-called "episodic" or "ballistic" jets (e.g., Fig. 1.5), which are different from the jets considered for the fundamental plane (for a discussion see [19]).

In summary, theory and numerical simulations suggest strongly that relativistic jets are powered by black hole spin, i.e., by a generalized Penrose process. However, observational evidence is limited to that shown in Fig. 1.7 and is in comparison weak.
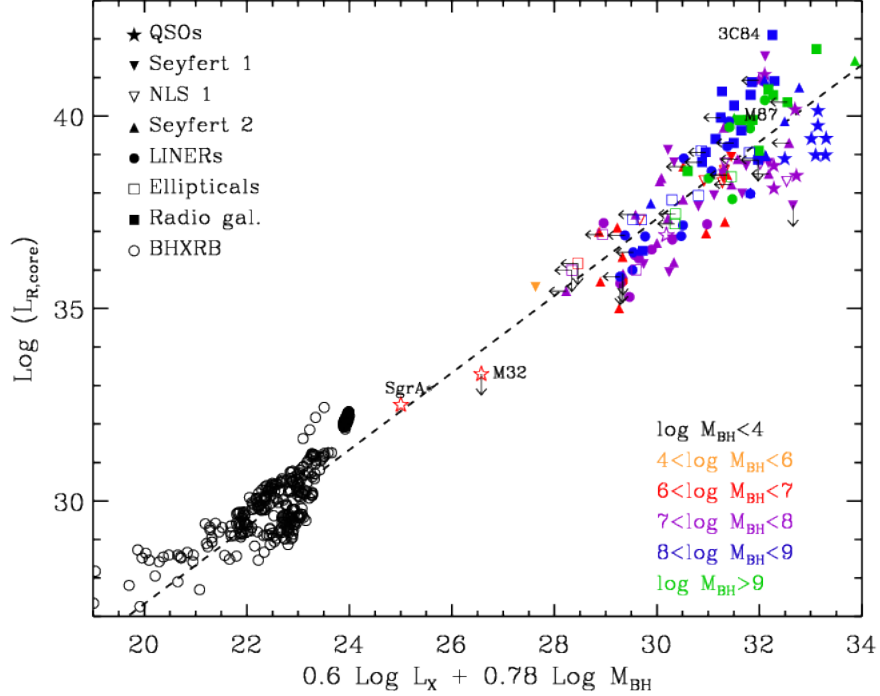
Figure 1.6 The "fundamental plane of black hole activity" [45]. The correlation extends over many decades of black hole mass and accretion luminosity, and includes many different source types. (Figure courtesy of A. Merloni.)

1.4.3 Testing the No-Hair Theorem

The No-Hair Theorem states that stationary black holes, such as those discussed herein, are completely described by the Kerr metric, which has only two parameters: black hole mass M and spin parameter a_*.[1] Testing this theorem requires measuring M and a_* of a black hole with great accuracy and demonstrating that no additional parameter is needed to explain any observable. At the present time, mass and spin measurements of stellar-mass and supermassive black holes are not accurate enough, nor are there a sufficient number of independent observables, to permit such a test.

The most promising system for testing the No-Hair Theorem is Sgr A*, the supermassive black hole in our Galaxy (§1.2.2). Within the next decade, ultra-high resolution interferometric observations are planned at millimeter

---

[1] In principle, a black hole can have a third parameter, electric charge, but the black holes studied in astrophysics are unlikely to have sufficient charge to be dynamically important.
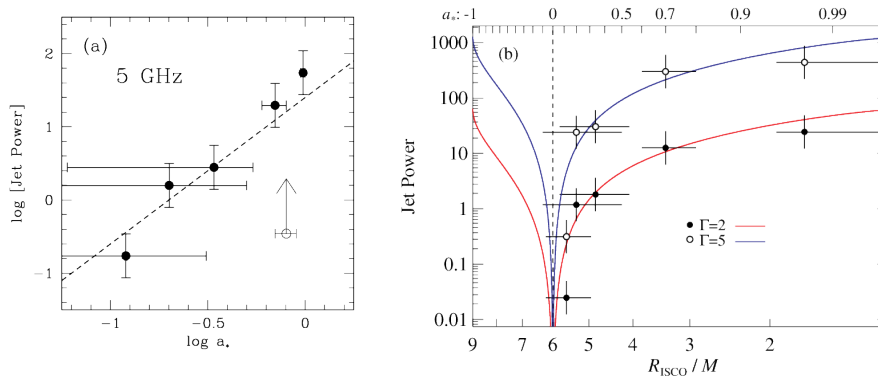
Figure 1.7 (a) Plot of jet power, estimated from 5 GHz radio flux at light curve maximum, versus black hole spin, measured via the continuum-fitting method, for five transient stellar-mass black holes [50, 74]. The dashed line has slope fixed to 2 (as predicted by theoretical models [5]) and is not a fit. (b) Plot of jet power versus R_{ISCO}/R_g. Here jet power has been corrected for beaming assuming jet Lorentz factor $\Gamma = 2$ (filled circles) or $\Gamma = 5$ (open circles). The two solid lines correspond to fits of a relation of the form "Jet Power" $\propto \Omega_H^2$, where Ω_H is the angular frequency of the black hole horizon. Note that the jet power varies by a factor of $\sim 10^3$ among the five objects shown.

wavelengths with the "Event Horizon Telescope" [15], which will produce direct images of the accreting gas in Sgr A* on length scales comparable to the horizon. These measurements could potentially be used to test the No-Hair Theorem (e.g. [35]).

1.5 Conclusion

The dawning that black holes are real occurred at the midpoint of this century of General Relativity, at the First Texas Symposium on Relativistic Astrophysics in 1963. There, Roy Kerr announced his solution, Jesse Greenstein described Maarten Schmidt's discovery of quasars, and Harlan Smith reported on the rapid variability of these objects [69]. Today, black hole astrophysics is advancing at a breathtaking rate. Tomorrow, spurred on by the commissioning of the Event Horizon Telescope and the advent of gravitational wave astronomy, it is reasonable to expect the discovery of many new unimaginable wonders.

References

[1] Abramowicz, M. A., Kluźniak, W. and Lasota, J.-P. 2002. No observational proof of the black-hole event horizon. *A&A*, **396**, L31–L34.

[2] Baade, W. and Minkowski, R. 1954. Identification of the radio sources in Cassiopeia, Cygnus A, and Puppis A. *ApJ*, **119**, 206–214.

[3] Bardeen, J. M., Carter, B. and Hawking, S. W. 1973. The four laws of black hole mechanics. *Comm. Math. Phys.*, **31**, 161–170.

[4] Bardeen, J. M., Press, W. H. and Teukolsky, S. A. 1972. Rotating black holes: Local nonrotating frames, energy extraction and scalar synchrotron radiation. *ApJ*, **178**, 347–370.

[5] Blandford, R. D. and Znajek, R. L. 1977. Electromagnetic extraction of energy from Kerr black holes. *MNRAS*, **179**, 433–456.

[6] Bolton, C. T. 1972. Identification of Cygnus X–1 with HDE 226868. *Nature*, **235**, 271–273.

[7] Bowyer, S., Byram, E. T., Chubb, T. A. and Friedman, H. 1965 Cosmic X-ray sources. *Science*, **147**, 394–398.

[8] Broderick, A. E., Loeb, A. and Narayan, R. 2009. The event horizon of Sagittarius A∗. *ApJ*, **701**, 1357–1366.

[9] Cantrell, A. G., Bailyn, C. D., Orosz, J. A., et al. 2010. The Inclination of the Soft X-Ray Transient A0620–00 and the Mass of its Black Hole. *ApJ*, **710**, 1127–1141.

[10] Charles, P. A. and Coe, M. J. 2006. Optical, ultraviolet and infrared observations of X-ray binaries. In *Compact stellar X-ray sources*, eds. W. H. G. Lewin and M. van der Klis, 215–265.

[11] Davis, S. W., Narayan, R., Zhu, Y., et al. 2011. The cool accretion disk in ESO 243–49 HLX–1: Further evidence of an intermediate-mass black hole. *ApJ*, **734**, 111 (10pp).

[12] Dai, S., Kochanek, C. S., Chartas, G., et al. 2010. The sizes of the X-ray and optical emission regions of RXJ 1131–1231. *ApJ*, **709**, 278–285.

[13] Di Matteo, T., Springel, V. and Hernquist, L. 2005. Energy input from quasars regulates the growth and activity of black holes and their host galaxies. *Nature*, **433**, 604–607.

[14] Doeleman, S. S., Weintroub, J., Rogers, A. E. E., et al. 2008. Event-horizon-scale structure in the supermassive black hole candidate at the Galactic Center. *Nature*, **455**, 78–80.

[15] Doeleman, S., Agol, E., Backer, D., et al. 2008. Imaging an event horizon: submm-VLBI of a supermassive black hole. Astro2010: The Astronomy and Astrophysics Decadal Survey, Science White Papers, No. 68 (arXiv:0906.3899 [astro-ph.HE]).

[16] Fabian, A. C., Iwasawa, K., Reynolds, C. S. and Young, A. J. 2000. Broad iron lines in active galactic nuclei. *Publ. Astron. Soc. Pacific*, **112**, 1145–1161.

[17] Fabian, A. C., Rees, M. J., Stella, L., et al. 1989. X-ray fluorescence from the inner disc in Cygnus X–1. *MNRAS*, **238**, 729–736.

[18] Falcke, H., Körding, E. and Markoff, S. 2004. A scheme to unify low-power accreting black holes. Jet-dominated accretion flows and the radio/X-ray correlation. *A&A*, **414**, 895–903.

[19] Fender, R. P. and Belloni, T. M. 2004. GRS 1915+105 and the disc-jet coupling in accreting black hole systems. *ARAA*, **42**, 317–364.

[20] Feng, H. and Kaaret, P. 2010. Identification of the X-ray thermal dominant state in an ultraluminous X-ray source in M82. *ApJL*, **712**, L169–L173.

[21] Ferrarese, L. and Merritt, D. 2000. A fundamental relation between supermassive black holes and their host galaxies. *ApJ*, **539**, L9–L12.

[22] Fish, V. L., Doeleman, S. S., Beaudoin, C., et al. 2011. 1.3 mm wavelength VLBI of Sagittarius A*: Deterction of time-variable emission on event horizon scales. *ApJL*, **727**, L36–L41.

[23] Gebhardt, K., Bender, R., Bower, G., et al. 2000. A relationship between nuclear black hole mass and galaxy velocity dispersion. *ApJ*, **539**, L13–L16.

[24] Ghez, A. M., Salim, S., Horrnstein, S. D., et al. 2005. Stellar orbits around the Galactic Center black hole. *ApJ*, **620**, 744–757.

[25] Gou, L., McClintock, J. E., Liu, J., et al. 2009. A determination of the spin of the black hole primary in LMC X–1. *ApJ*, **701**, 1076–1090.

[26] Gou, L., McClintock, J. E., Reid, M. J., et al. 2011. The extreme spin of the black hole in Cygnus X–1. *ApJ*, **742**, 85 (17pp).

[27] Gou, L., McClintock, J. E., Steiner, J. F., et al. 2010. The spin of the black hole in the soft X-ray transient A0620–00. *ApJ*, **718**, L122–L126.

[28] Greene, J., Bailyn, C. D. and Orosz, J. A. 2001. Optical and infrared photometry of the microquasar GRO J1655–40 in quiescence. *ApJ*, **554**, 1290–1297.

[29] Greenhill, L. J., Jiang, D. R., Moran, J. M., et al. 1995. Detection of a subparsec diameter disk in the nucleus of NGC 4258. *ApJ*, **440**, 619–627.

[30] Hargrave, P. J. and Ryle, M. 1974. Observations of Cygnus A with the 5–km radio telescope. *MNRAS*, **166**, 305–327.

[31] Heinz, S. and Sunyaev, R. A. 2003. The non-linear dependence of flux on black hole mass and accretion rate in core-dominated jets. *MNRAS*, **343**, L59–L64.

[32] Hey, J. S., Parsons, S. J. and Phillips, J. W. 1946. Fluctuations in cosmic radiation at radio-frequencies, *Nature*, **158**, 234.

[33] Humphreys, E. M. L., Reid, M. J., Moran, J. M., et al. 2013. Toward a new geometric distance to the active galaxy NGC 4258. III. Final results and the Hubble constant. *ApJ*, **775**, 13 (10pp).

[34] Jennison, R. C. and Das Gupta, M. K. 1953. Fine structure of the extraterrestrial radio source Cygnus I. *Nature*, **172**, 996–997.

[35] Johannsen, T. and Psaltis, D. 2010. Testing the No-Hair Theorem with observations in the electromagnetic spectrum. II. Black hole images. *ApJ*, **718**, 446–454.

[36] Kalogera, V. and Baym, G. 1996. The maximum mass of a neutron star. *ApJ*, **470**, L61–L64.

[37] King, A. 2003. Black holes, galaxy formation, and the M_{BH}-σ relation. *ApJ*, **596**, L27–L29.

[38] King, A. 2005. The AGN-starburst connection, galactic superwinds, and M_{BH}-σ. *ApJ*, **635**, L121–L123.

[39] Kormendy, J. and Ho, L. C. 2013. Coevolution (or not) of supermassive black holes and host galaxies. *ARAA*, **51**, 511–653.

[40] Lasota, J.-P., Gourgoulhon, E., Abramowicz, M., et al. 2014. Extracting black-hole's rotational energy: The generalized Penrose process. *Phys. Rev. D*, **89**, 024041 (24pp)

[41] Liu, J.,McClintock, J. E., Narayan, R., et al. 2008. Precise measurement of the spin parameter of the stellar-mass black hole M33 X–7. *ApJ*, **679**, L37–L40 (Erratum: **719**, L109).

[42] Magorrian, J., Tremaine, S., Richstone, D., et al. 1998. The demography of massive dark objects in galaxy centers. *AJ*, **115**, 2285–2305.

[43] McClintock, J. E., Narayan, R. and Steiner, J. F. 2013. Black hole spin via continuum fitting and the role of spin in powering transient jets. *Space Sci. Rev.* (arXiv:1303.1583 [astro-ph.HE]).

[44] McClintock, J. E., Shafee, R., Narayan, R., et al. 2006. The spin of the near-extreme Kerr black hole GRS 1915+105. *ApJ*, **652**, 518–539.

[45] Merloni, A., Heinz, S. and di Matteo, T. 2003. A fundamental plane of black hole activity. *MNRAS*, **345**, 1057–1076.

[46] Meyer, L., Ghez, A. M., Schödel, R., et al. 2012. The shortest-known-period star orbiting our Galaxy's supermassive black hole. *Science*, **338**, 84–87.

[47] Mirabel, I. F. and Rodriguez, L. F. 1994. A superluminal source in the Galaxy. *Nature*, **371**, 46–48.

[48] Miyoshi, M., Moran, J., Herrnstein, J., et al. 1995. Evidence for a black hole from high rotation velocities in a sub-parsec region of NGC4258. *Nature*, **373**, 127–129.

[49] Narayan, R. and McClintock, J. E. 2008. Advection-dominated accretion and the black hole event horizon. *NewAR*, **51**, 733–751.

[50] Narayan, R. and McClintock, J. E. 2012. Observational evidence for a correlation between jet power and black hole spin. *MNRAS*, **419**, L69–L73.

[51] Novikov, I. D. and Thorne, K. S. 1973. Astrophysics of black holes. In *Black Holes (Les Astres Occlus)*, ed. A. Giannaras, 343–450.

[52] Orosz, J. A., McClintock, J. E., Aufdenberg, J. P., et al. 2011a. The mass of the black hole in Cygnus X–1. *ApJ*, **742**, 84 (10pp).

[53] Orosz, J. A., McClintock, J. E., Narayan, R., et al. 2007. A 15.65-solar-mass black hole in an eclipsing binary in the nearby spiral galaxy M 33. *Nature*, **449**, 872–875.

[54] Orosz, J. A., Steeghs, D., McClintock, J. E., et al. 2009. A new dynamical model for the black hole binary LMC X–1. *ApJ*, **697**, 573–579.

[55] Orosz, J. A., Steiner, J. F., McClintock, J. E., et al. 2011b. An improved dynamical model for the microquasar XTE J1550–564. *ApJ*, **730**, 75 (13pp).

[56] Özel, F., Psaltis, D., Narayan, R., et al. 2010. The black hole mass distribution in the Galaxy. *ApJ*, **725**, 1918–1927.

[57] Penna, R. F., Narayan, R. and Sadowski, A. 2013. General relativistic magnetohydrodynamic simulations of Blandford-Znajek jets and the membrane paradigm. *MNRAS*, **436**, 3741–3758.

[58] Penrose, R. 1969. Gravitational collapse: The role of general relativity *Riv. Nuovo Cim.*, **I**, 252.

[59] Peterson, B. M., Ferrarese, L., Gilbert, K. M., et al. 2004. Central masses and broad-line region sizes of active galactic nuclei. II. A homogeneous analysis of a large reverberation-mapping database *ApJ*, **613**, 682–699.

[60] Reber, G. 1944. Cosmic static. *ApJ*, **100**, 279–287.

[61] Reid, M. J. and Brunthaler, A. 2004. The proper motion of Sagittarius A*. II. The mass of Sagittarius A*. *ApJ*, **616**, 872–884.

[62] Remillard, R. A. and McClintock, J. E. 2006. X-ray properties of black-hole binaries. *ARAA*, **44**, 49–92.

[63] Reynolds, C. S. 2013. Measuring black hole spin using X-ray reflection spectroscopy. *Space Sci. Rev.* (arXiv:1302.3260 [astro-ph.HE]).

[64] Rhoades, C. E. and Ruffini, R. 1974. Maximum mass of a neutron star *PhRvL*, **32**, 324–327.

[65] Ruffini, R. and Wilson, J. R. 1975. Relativistic magnetohydrodynamical effects of plasma accreting into a black hole. *Phys. Rev. D*, **12**, 2959–2962.

[66] Russell, D. M., Gallo, E. and Fender, R. P. 2013. Observational constraints on the powering mechanism of transient relativistic jets. *MNRAS*, **431**, 405–414.

[67] Schmidt, M. 1963. 3C 273: A star-like object with large redshift. *Nature*, **197**, 1040.

[68] Schödel, R., Ott, T., Genzel, R., et al. 2002. A star in a 15.2 year orbit around the supermassive black hole at the center of the Milky Way *Nature*, **419**, 694–696.

[69] Schucking, E. L. 1989. The first Texas Symposium on relativistic astrophysics. *Phys. Today*, **42**, 46–52.

[70] Shafee, R., McClintock, J. E., Narayan, R., et al. 2006. Estimating the spin of stellar-mass black holes by spectral fitting of the X-Ray continuum. *ApJ*, **636**, L113–L116.

[71] Shakura, N. I. and Sunyaev, R. A. 1973. Black holes in binary systems. Observational appearance. *A&A*, **24**, 337–355.

[72] Smith, F. G. 1951. An accurate determination of the positions of four radio stars. *Nature*, **168**, 555.

[73] Steeghs, D., McClintock, J. E., Parsons, S. G., et al. 2013. The not-so-massive black hole in the microquasar GRS1915+105. *ApJ*, **768**, 75 (7pp).

[74] Steiner, J. F., McClintock, J. E. and Narayan, R. 2013. Jet power and black hole spin: Testing an empirical relationship and using it to predict the spins of six black holes. *ApJ*, **762**, 104–113.

[75] Steiner, J. F., Reis, R. C., McClintock, J. E., et al. 2011. The spin of the black hole microquasar XTE J1550–564 via the continuum-fitting and Fe-line methods. *MNRAS*, **416**, 941–958.

[76] Tanaka, Y., Nandra, K., Fabian, A. C., et al. 1995. *Nature*, **375**, 659–661.

[77] Tananbaum, H., Gursky, H., Kellogg, E., et al. 1972. Observations of a correlated X-ray transition in Cygnus X–1. *ApJ*, **177**, L5–L10.

[78] Tchekhovskoy, A., Narayan, R. and McKinney, J. C. 2011. Efficient generation of jets from magnetically arrested accretion on a rapidly spinning black hole. *MNRAS*, **418**, L79–L83.

[79] van Velzen, S. and Falcke, H. 2013 The contribution of spin to jet-disk coupling in black holes. *A&A*, **557**, L7 (4pp).

[80] Vestergaard, M. and Peterson, B. M. 2006. Determining central black hole masses in distant active galaxies and quasars. II. Improved optical and UV scaling relationships. *ApJ*, **641**, 689–709.

[81] Webster, B. L. and Murdin, P. 1972. Cygnus X–1 — A spectroscopic binary with a heavy companion? *Nature*, **235**, 37–38.

[82] Zhang, S. N., Cui, W. and Chen, W. 1997. Black hole spin in X-ray binaries: Observational consequences. *ApJL*, **482**, L155–L158.